Using lateral capillary forces to compute by self-assembly

Paul W. K. Rothemund[†]

University of Southern California, Laboratory for Molecular Science, Los Angeles, CA 90089-1340

Edited by George M. Whitesides, Harvard University, Cambridge, MA, and approved December 13, 1999 (received for review September 21, 1999)

Investigations of DNA computing have highlighted a fundamental connection between self-assembly (SA) and computation: in principle, any computation can be performed by a suitable self-assembling system. In practice, exploration of this connection is limited by our ability to control the geometry and specificity of binding interactions. Recently, a system has been developed that uses surface tension to assemble plastic tiles according to shape complementarity and likeness of wetting [Bowden, N., Terfort, A., Carbeck, J. & Whitesides, G. M. (1997) *Science* 276, 233–235]. Here the capacity of this system to compute by SA is explored. Tiles were prepared to test the system's ability to generate three structures of increasing complexity: a periodic checkerboard tiling, an aperiodic Penrose tiling, and a computational tiling that simulates a one-dimensional cellular automaton. Matching rules for these tilings were enforced by coating tiles with patterns of hydrophobic and hydrophilic patches or wetting codes. Energetic, kinetic, and mechanistic details of SA explain differences between experimental structures and mathematically ideal ones. In particular, the growth mechanism observed appears incompatible with computations that make use of a chosen input.

Self-assembly (SA) and computation are linked by the study of mathematical tiling (1). A tiling is an arrangement of tiles (shapes) that covers the plane. Tiles fit together according to matching rules: their edges must have complementary shapes and must agree on additional markings such as colors. Given any computing device (e.g., a Turing machine, ref. 2, or cellular automaton), tiles and matching rules can be designed so that the tilings formed correspond to a simulation of that device (typically, successive rows in the tiling represent the memory of the device at successive time steps). Computation by tiling is thus universal.

Tiles, matching rules, and the tilings they define are abstract mathematical objects but their geometrical natures suggest physical analogues. Real objects (e.g., atoms) may be thought of as tiles, binding interactions (e.g., chemical bonds) as matching rules, and self-assembled structures (e.g., molecules) as partial tilings. Such an analogy has been used to describe the structure of quasicrystals in terms of Penrose (P) tilings (3).

Together, the connection of computation to mathematical tiling and analogies between tiling and SA imply that, in principle, any computation can be realized as a self-assembled structure. Conversely, the Church–Turing thesis implies that all self-assembled structures can be viewed as computations. Why study such connections? Originally, in the context of DNA computation, the purpose was to perform computation and compete with electronic computers. DNA SA has been used in the solution of an NP-complete problem (4) and to create two-dimensional DNA lattices (5) as a step toward simulating cellular automata (6). Competing with electronic computers is a difficult goal, one that seems unlikely to be met. Rather, the link between computation and SA may find most use in defining the structures accessible by SA, both theoretically and practically. Theoretically because the mathematics of computation may be used to classify self-assembled structures (e.g., to map self-assembled structures onto languages in the Chomsky hierarchy, ref. 6) or to analyze the resources, in terms of time or tile complexity, needed to create a particular structure (e.g., to find the smallest number of tile species that assemble uniquely into an *nxn* square, E. Winfree and P.W.K.R., unpublished work). Practically because tilings that encode computations provide new synthetic targets—structures more complex, in general, than any considered by chemists so far. Often they are nonperiodic and require many distinct binding interactions. Thus assembly of "computational" tile sets may test the limits of synthesis by SA. [The structure created by any set of tiles can be interpreted as a computation; so, too, can the operation of any machine. Still, one neither refers to all tile sets as computational nor calls all machines computers. The adjective computational, like the term computer itself, connotes intent to perform a computation of interest, or of particular power.] Here such practical issues are explored.

The smallest number of binding interactions that allows universal computation is not known, but straightforward encodings of many computations require a dozen or more (e.g., enumerating primes, ref. 1), suggesting DNA as the best medium for making such structures. Recently, capillary force-based systems (7–9) have become alternatives. Like DNA, these systems allow many binding interactions; unlike DNA, they allow easy control of tile geometry and visual inspection of reaction mechanism. Capillary force SA operates on particles as small as 55 nm (10), and proteins a few nm in size appear to assemble by capillary forces in lipid bilayers (11). Thus capillary force SA may allow microfabrication of computational tilings. Here I show that such a system is rich enough to enforce four matching rules—sufficiently many to make tiles encoding a simple binary function, exclusive-or (XOR), and simulate a one-dimensional cellular automaton to create triangular patterns.

Unfortunately, simply creating binding interactions to enforce matching rules does not ensure that tiles assemble as desired. Antithetical to most chemists' idea of good rational design, distinct tiles may bear the same matching rule and compete for a single lattice site. I term a tile set competitive if it can form a lattice site such that one tile is correct (matching the site on all sides), and another tile competes and is incorrect (matching and mismatching the site on at least one side). Natural encodings of computations as tiles often yield competitive tile sets (1), and an important open question is: Are competitive tile sets required for universal computation? For such tiles, error-free assembly requires that binding be cooperative. I define binding to be cooperative if the equilibrium constant for association of a tile at a site increases strictly with the number of bonds the tile can make with that site. For experiments reported here cooperative binding appears responsible for an error rate ≈6-fold lower than noncooperative binding would predict. Finally, for many computational tile sets, specifying a particular computation requires

This paper was submitted directly (Track II) to the PNAS office.

Abbreviations: SA, self-assembly; C, checkerboard; P, Penrose; XOR, exclusive-or; IS, ideal structure; F, hydrophobic; L, hydrophilic; WC, wetting code.

[†]To whom reprint requests should be addressed. E-mail: rothemun@pollux.usc.edu.

The publication costs of this article were defrayed in part by page charge payment. This article must therefore be hereby marked "*advertisement*" in accordance with 18 U.S.C. §1734 solely to indicate this fact.

that tiles bind into corner sites on a special input tile. Here tiles are observed to bind by a mechanism that precludes computation using such a chosen input.

Materials and Methods

Ideal Structures (ISs) and Simulations. Wulff's rule (12) gives a square IS for checkerboard (C) or XOR tiles and a decagonal IS (13) for P tiles (14). The P tile IS given is approximate. Simulations were initialized by assigning a random position to each tile (168 C tiles, 420 P tiles, 256 XOR tiles) in a square space (discrete for C and XOR tiles, continuous for P tiles) of a size (25, 31, or 27 tile widths wide, respectively) chosen to match the dimensions of the SA experiments described below. Each step, one structure (collection of one or more tiles connected by bonds) was chosen at random and moved one tile width in a random direction (up, down, right, or left) if no overlap occurred with other tiles. [P tiles were moved with a displacement chosen randomly from [0,2) and a 66% chance of rotation ± 36°.] Any collision of the moved structure with stationary ones for which the edges involved satisfied a matching rule caused the creation of a bond. Each simulation continued until all tiles joined a single structure or 2,000 moves passed without formation of a bond. On average ($n = 40$), simulations terminated in ≈1,400, 6,000, or 900 steps leaving 1.1, 5.2, or 1.1 structures for C, P, or XOR tiles, respectively.

Preparation of Tiles. All tiles were laser-cut (ULS 25, Universal Laser Systems, Scottsdale, AZ) from 3-mm fluorescent yellow cast acrylic (Solter Plastics, Los Angeles). Before cutting, the bottom of the acrylic was made hydrophilic (L) by wetting it with cyanoacrylate ester (Zap-O, Pacer Technology, Rancho Cucamonga, CA) and dusting with silica gel (type G, Sigma) three times. The top of the acrylic was sprayed fluorescent blue. Patterns indicating matching rules were created by burning away paint at a low power setting. Notches (1 mm deep, 0.2 mm wide) were cut between regions to be made hydrophobic (F) or L. Tiles were cut from the acrylic sheet at a high power setting, stacked, and covered in tape. Using the notches as guides, tape was cut away from regions to be made L. The resulting stacks of tiles were wet with cyanoacrylate and dusted with silica three times, yielding a layer of cyanoacrylate/silica ≈ 0.1 mm thick. F patches were deprotected and painted with fluid (naptha, butadiene rubber, butyl Cellosolve) from an F slide marker (PAP Pen, RPI, Mount Prospect, IL) diluted 7:1 in hexane.

Visualization of the Meniscus. F sand (CENCO, Franklin Park, IL) was sprayed with red fluorescent paint. Visualization of L patches was performed by adding 30 mg sand/cm^2 interface between mineral oil (Aldrich, 0.83 g/ml) and aqueous sodium metatungstate (Geoliquids, Prospect Heights, IL, 1.65 g/ml).

SA. All experiments used an *n*-hexadecane (Sigma, 0.77 g/ml) superphase and an aqueous sodium metatungstate subphase. Tiles were shaken with an AROS 160 shaker (Barnstead-Thermolyne, 3.8-cm orbit). Before use, tiles were soaked 30 min in water. The tiles in Fig. 2 were placed in a 10-cm square box with 100 ml of subphase and 50 ml of superphase, disaggregated with forceps while shaken at 78 rpm so that ≈50% of bonds were broken, and equilibrated at 75 rpm. The ratio of L/F bonds was stable after 30 s but data were taken after 5 min. C tiles were shaken in an 18-cm square glass dish with 120 ml of superphase and 120 ml of subphase (1.65 g/ml) for 5 min at 44.5 rpm, 15 min at 40.9 rpm, 45 min at 37.6 rpm, 135 min at 34.0 rpm, 405 min at 30.6 rpm, and 1,215 min at 27.0 rpm. P tiles were shaken in a 38-cm square glass box with 450 ml of superphase and 1,100 ml of subphase (1.65 g/ml) for 3 h at 22.6 rpm, 6 h at 21.8 rpm, 12 h at 21.1 rpm, 24 h at 20.5 rpm, 48 h at 19.8 rpm, 48 h at 19.0 rpm, 24 h at 18.3 rpm, 24 h at 17.6 rpm, and 24 h at 16.9 rpm. XOR tiles were shaken in a 32-cm square glass box with 220 ml of superphase and 860 ml of subphase (1.65 g/ml) for 12 h at 23.7 rpm, 24 h at 21.8 rpm, and 24 h at 18.3 rpm.

Results and Discussions

ISs, Simulations, and Prerequisites for Computation. Modeling suggests (*i*) under a given set of growth rules for SA, certain tile sets are particularly prone to form defects and (*ii*) for a particular tile set different growth rules yield structures of very different quality. This raises two questions: (*i*) Will tile sets that encode computations be, in general, prone to defect formation? (*ii*) If so, what growth rules must SA follow so that such tile sets self-assemble successfully? To explore these questions I compare the hypothetical and experimental SA of a competitive set of computational tiles (XOR tiles, Fig. 1*I*) with two simpler sets of tiles: C tiles (Fig. 1*A*) and P tiles (Fig. 1*E*). XOR tiles were studied because competitive tile sets with the same form (two inputs and a one duplicated output) exist that are universal (from the universality of one-way cellular automaton, ref. 15). Thus if conditions for correct XOR tile assembly can be found, any computation can be performed.

For each set of tiles an IS is given (Fig. 1 *B*, *F*, and *J*), intuitively an example of the best one could expect SA to produce. An IS is, for a fixed number of tiles, one of many structures that minimize unmatched edges and violate no matching rules. For comparison, structures (Fig. 1 *C*, *G*, and *K*) were created by simulation using a model of SA (16) where binding is irreversible. These structures are far from ideal: dendritic rather than compact, having only ≈60% of the bonds (matched edge pairs) present in the ISs, and bearing vacancy defects and errors (sites where abutting edges mismatch). Strikingly, error rates range over almost 2 orders of magnitude: 0.2%, 2.2%, and 14.7% for C, P, and XOR tiles, respectively (% error = mismatches/[mismatches + bonds]).

Diagrams of bond formation (Fig. 1 *D*, *H*, and *L*) contrast error-formation mechanisms for the three tile sets. Only mechanisms involving monomers are shown, but analogous mechanisms involving multi-tile structures also occur. C tiles made errors only when a structure was mechanically trapped in a larger structure (Fig. 1*D*, tile t); no bonds held such a tile in the lattice. No P tiles and few XOR tiles were trapped; for them errors (100%, >99%) resulted from association of a tile (or larger structure) matching the lattice on one edge but mismatching on another (Fig. 1 *H* and *L*, *). P tiles made such errors when incompletable sites (for which no tile with correct matching rules for both sides of the site exists, Fig. 1*H*, inc) were filled. XOR tiles did form and fill incompletable sites but many errors formed because XOR tiles are competitive: at a single site a correct tile (Fig. 1*L*, d) that binds by two bonds competes with two incorrect tiles (Fig. 1*L*, s) that bind by single bonds.

A tendency for P tiles (17) and tiles similar to XOR tiles (18) to form defects has been noted before and raises questions of whether (*i*) SA of P tiles models the formation of well-ordered quasicrystals and (*ii*) SA of XOR tiles can perform error-free computation. In fact, the SA of P and XOR tiles is highly growth rule dependent. Conditions for nearly defect-free assembly of P tiles are complex and are treated elsewhere (19, 20).

To understand conditions sufficient for XOR tiles to assemble without defects and compute as desired, consider first how they compute (see legend for Fig. 1 *I* and *L*). If tiles are labeled 0 or 1 based on the identity of their output bits, a row of tiles can be read as a string of binary digits that represent the memory cells of a one-dimensional blocked cellular automaton at a single time step in its simulation. The next row (immediately above) represents the memory cells in the next time step where each memory cell in the next row is the XOR of two neighboring cells. The IS in Fig. 1*J* is then a fragment of a random computation, the result of simulating the blocked cellular automaton on a random binary

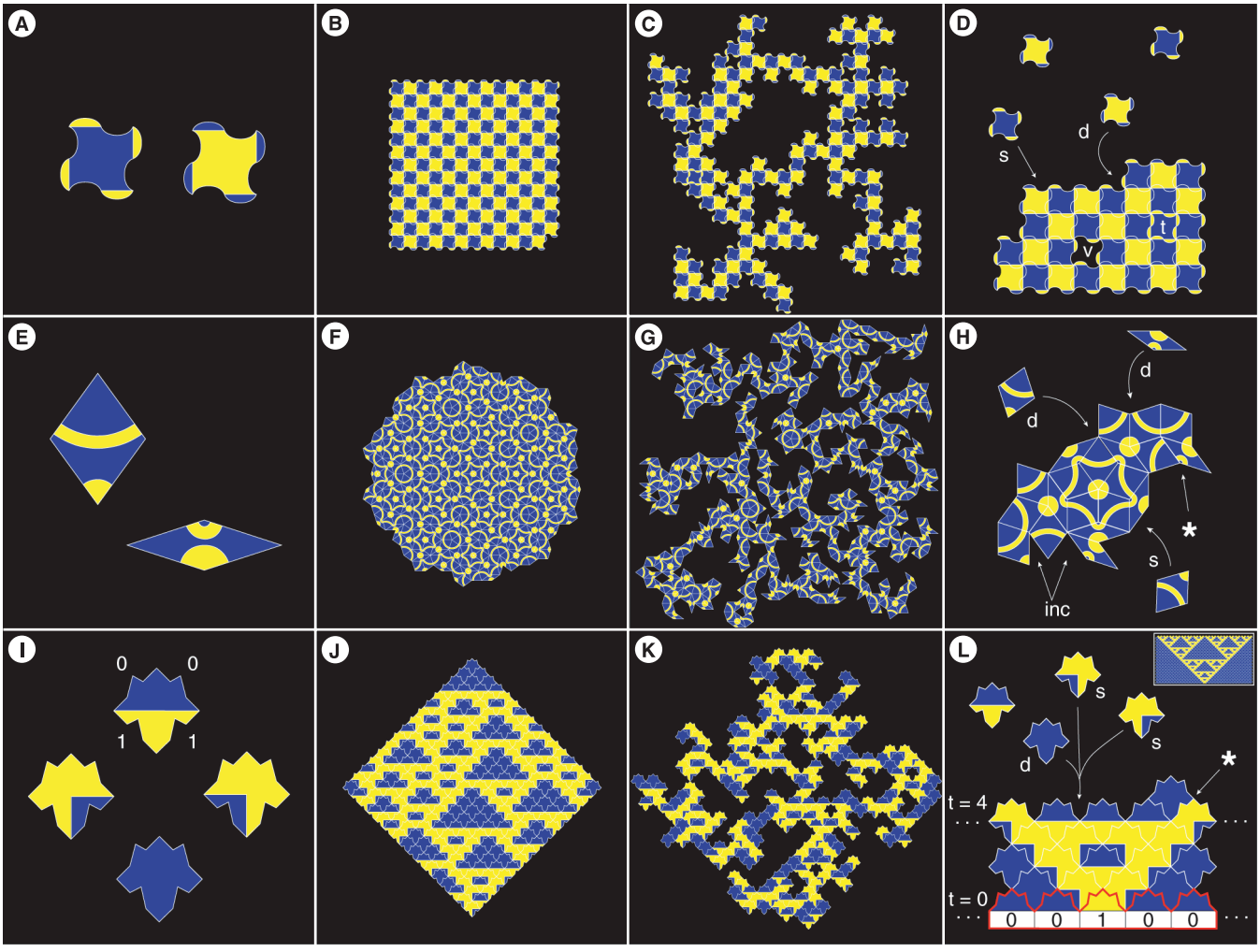

Fig. 1. Tiles, ISs, and structures formed by simulation. (*A*) C tiles. (*B*) Periodic IS with a minimal number of unmatched edges. (*C*) Simulation results. Few errors (0.2% of abutting edges are mismatched, $n = 40$) but many unbound edges are present. (*D*) Schematic shows tiles binding by a single (s) bond along a face or by a double (d) bond into a corner. Errors form only by mechanical trapping (t). Vacancies (v) also form. (*E*) P tiles. (*F*) Aperiodic IS (approximate). (*G*) Simulation results. A moderate number of errors (2.2%) and three separate structures are present. (*H*) Schematic shows tiles binding by single (s) or double (d) bonds. Matching rules allow incompletable sites (inc) into which no tile can fit without error (*), which occurs when such a site is filled. (*I*) XOR tiles encode the binary function XOR ($X \oplus Y = Z$). Concave lower edges denote a pair of input bits X and Y (yellow = 1, blue = 0). Convex upper edges denote two copies of an output bit Z. The top tile encodes $1 \oplus 1 = 0$, the leftmost tile $1 \oplus 0 = 1$, the rightmost tile $0 \oplus 1 = 1$ and the bottom tile $0 \oplus 0 = 0$. (*J*) IS. (*K*) Simulation results (rotated 45° for viewing convenience). Many errors (14.7%) are present. (*L*) Schematic shows XOR tiles assembling on an input tile, outlined in red, denoting the string 00100 continued on both sides with zeros. Successive rows correspond to successive time steps ($t = 0 \ldots t = 4$) in a simulation of the corresponding one-dimensional blocked cellular automaton (ref. 25, rule 60). Arrow indicates three tiles competing for a corner site, two of which (s) would form an error (*) if incorporated. (*Inset*) A larger, perfect section of the intended structure, Pascal's triangle mod 2.

string. Fig. 1*L* shows the beginning of a specific computation where the assembly of XOR tiles has been nucleated on an input tile, a long special tile that provides a chosen input to the computation. In this case XOR tiles would form Pascal's triangle mod 2 (*Inset* Fig. 1*L*), an example where computational tiles provide a striking synthetic target—a discrete approximation of the Sierpinski triangle fractal. Without such nucleation, all possible computations are created and a particular computation of width n would be just one of 2^n competing structures similar to Fig. 1*J*. Trivially, to achieve such nucleation, tiles must bind corners (sites comprising a pair of perpendicular edges). Additionally, assuming that tiles can bind to a lattice via a single bond: (*i*) Tiles must bind reversibly so that vacancies, incompletable sites, and errors can be resolved. (*ii*) Associations must be cooperative (a tile that matches a corner on both edges must be preferred over a tile that matches on one edge) so that errors are infrequent. Two types of incorrect tile compete with one type of correct tile for a corner site; without cooperative binding each would bind (and dissociate) equally often, yielding an error rate of 1/3 (33%). With cooperative binding correct tiles dissociate at a lower rate than incorrect tiles; if the strength of a single bond is $\Delta G < 0$, the preference of a correct tile over an incorrect one at equilibrium is $e^{-\Delta G/RT}$ (21) so, in principle, very low error rates can be achieved.

Physical Implementation. To create real tiles analogous to those in Fig. 1, the system described in ref. 11 was used. Millimeter-scale tiles floating between an F and an L phase deform the interface by trapping it above or below its equilibrium height. This happens wherever the side of a tile with F character protrudes into the L phase and vice versa (Fig. 2 *A–C*). Capillary forces between tiles are attractive or repulsive, respectively, if movement of the tiles decreases or increases the area, and hence the energy, of the interface (22). When a vessel containing such a

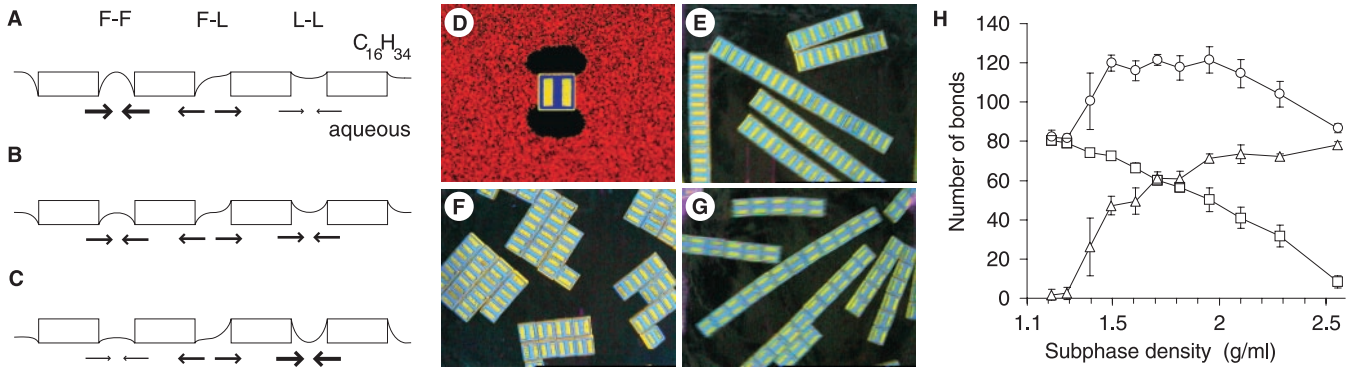

Fig. 2. Changes in SA as a function of subphase density (ρ, given in g/ml). (*A–C*) Side views diagram menisci between tiles at the interface of a hexadecane superphase ($C_{16}H_{34}$) and aqueous sodium metatungstate subphases (aqueous) of increasing density. Tiles (*A*) sink deeply into a dilute subphase, (*B*) rest halfway between phases on a more concentrated subphase, and (*C*) ride high on a saturated subphase. F–F, F–L, and L–L indicate the meniscus between F and/or L tiles. Tiles move to minimize the area, and hence energy, of the interface. Arrows give the direction and, for attraction, relative strength of the force between tiles. (*D*) Top view of a 5-mm square tile with one pair of opposing faces made L and the other made F. The interface has been doped with F sand that moves away from L sides and toward F sides to show lines of constant height in the meniscus. (*E–G*) Assembly under conditions analogous to *A–C* with $\rho = 1.3$ (*E*), 1.71 (*F*), or 2.4 (*G*). Note different tile orientations in *E* and *G*. (*H*) Number of L and F bonds plotted as a function of ρ. Error bars are: 1 SD. L bonds (Δ) dominate for $\rho >$ 1.71; F bonds (□) dominate for $\rho < 1.71$. The total number of bonds (○) is roughly constant from $\rho = 1.49$ to 1.95. Bond strengths are equal for $\rho = 1.71$, close to the density ($\rho = 1.65$) predicted.

system is shaken on a rotary shaker, tiles with strong interactions form and maintain stable associations termed bonds. Binding is reversible; shaking at higher frequencies causes bond equilibria to shift toward dissociation. Thus shaking is an analogue for temperature. Tiles were shaken with a decreasing frequency profile to anneal structures toward the ISs given in Fig. 1.

Enforcing the matching rules given in Fig. 1 requires the use of up to four (for XOR tiles) different binding interactions that must be specific and isoenergetic. Specificity may be conferred by giving tiles complementary shapes or patterns of wetting (8). Attempts to make binding interactions based entirely on shape failed (not shown) because noncomplementary shapes had binding energies too similar to complementary ones. To overcome this I introduced patterns of alternating L and F patches or wetting codes (WCs) to enforce matching rules and made limited use of shape.

The design of good WCs is subject to constraints that derive from both the logic of the matching rules and the physics of the system. Conceptually, it was useful to view WCs as binary strings. The Hamming distance (number of mismatches) between pairs of codes could then be optimized. Wherever possible, Hamming distances for mismatches were made greater than half the length of the code. This insured that mismatches were actually repulsive. Self-interactions were avoided by making WCs nonpalindromic. Finally, for WCs applied to straight edges, care was taken to minimize shifted alignments of the edges with many unintended matches in wetting character.

Yet physics dictates that one cannot treat L and F patches merely as zeros and ones. An uneven distribution of L and F patches around the perimeter of a tile may cause it to tilt (9) and inhibit aggregation. Further, the degree of deformation of the interface along an edge (and hence bond strength) is not simply a function of the number of F and L patches. A sequence of patches induces a wave-like meniscus that changes curvature at each change in wetting character. The amplitude of this wave at a given patch is roughly the width of a patch (23) and is limited by the thickness of the tile. Consecutive patches of the same type are, effectively, part of one large patch. Thus a sequence F, F, L, L does not change the interfacial area in the same way as an F, L, F, L sequence. The use of sequences with a similar number and distribution of changes in wetting character should help minimize differences in meniscus deformation and create isoenergetic bonds. P tiles were not designed weighing this criterion heavily and the consequences are described later.

Another way to regularize the contribution of a patch to the interfacial tension is to equalize the strength of L and F interactions. In the previously described water/perfluorodecalin system (8), polydimethylsiloxane tiles float so that most of their thickness lies in the water superphase (upside down, but analogous to Fig. 2*A*). Thus in this system, F bonds are strong and L bonds are weak. Here acrylic tiles float between hexadecane and a sodium metatungstate solution. By changing the concentration of salt in the subphase, the equilibrium position of the tiles at the interface was adjusted. This allowed the strengths of L and F bonds to be equalized and a repulsive force between F and L patches to be maintained (Fig. 2*B*).

L and F bonds are equally strong when the tiles sit midway between the two phases. At this midway point, for a tile with an equal number of L and F patches, the capillary forces' contribution to its position cancels. Thus Archimedes' law was used to find the subphase density (1.65 g/ml) for which an acrylic tile (1.21 g/ml) sits midway between the hexadecane (0.77 g/ml) superphase and aqueous subphase. To test this, 5-mm square tiles were made so that one pair of opposing sides was L, and the other F as visualized in Fig. 2*D*. Tiles formed linear structures with F bonds (Fig. 2*E*) when shaken at low subphase densities, square structures with F and L bonds (Fig. 2*F*) at intermediate densities, or linear structures with L bonds (Fig. 2*G*) at high densities. The relative strength of the F and L bonds were measured (Fig. 2*H*) by shaking the tiles at a constant rate until the structures formed were in equilibrium and then counting F and L bonds. At the subphase density for which these numbers were equal (1.71 g/ml) the bond strengths were equal, in good agreement with prediction.

SA. To show the assembly of C tiles using a simple WC, two kinds of square tiles were prepared. The side of each tile bore a two-patch code, for which half of each side was made F and the other L (Fig. 3*A*). Tiles were disaggregated (Fig. 3*B*) and shaken for ≈30 h, after which structures (Fig. 3*C*) with a few vacancies were observed. The structures had 288 ± 8 bonds ($n = 4$)—92% of the 312 bonds in an approximately square IS. Fig. 3*D* shows shifted bonds—artifacts of the chosen WC common before annealing (Fig. 3*B*), but rare once annealing began.

P tile matching rules require two kinds of nonpalindromic

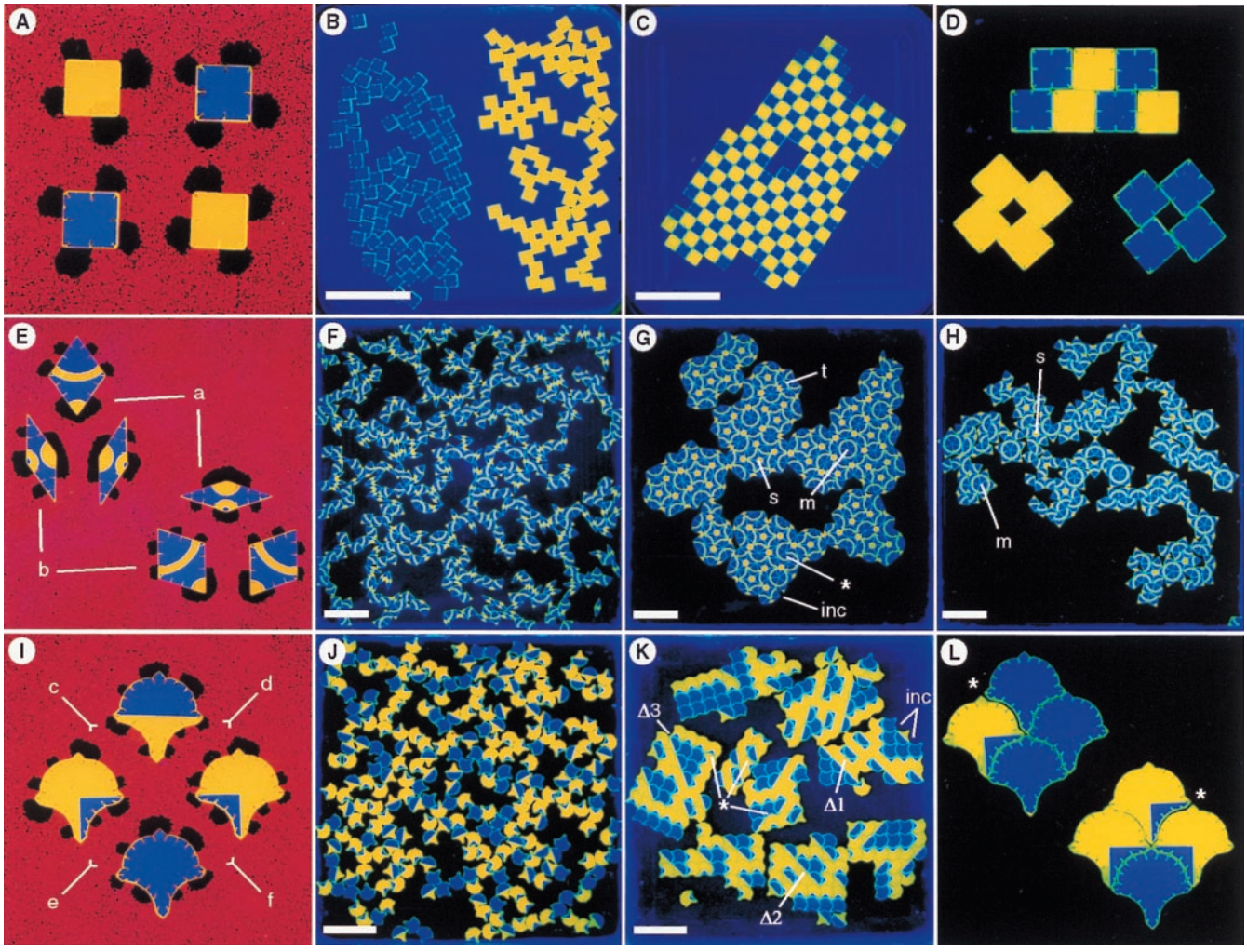

Fig. 3. SA of tiles with increasingly complex WCs. (Scale bars: 5 cm.) (*A–D*) C tiles, 7.5 mm square. (*A*) Visualization of L patches. (*B*) Disaggregated. (*C*) Shaken ≈30 h. (*D*) Shifted bonds are strongest at the extremes of subphase density (here 2.4 g/ml) but are present before shaking for all ρ. (*E–H*) P tiles, 1.2 cm on a side. (*E*) Two codes (a and b) are used. (*F*) Disaggregated. (*G*) Shaken ≈9 days. Note the common vertex star (s) whose moon isomer (m) occurs only once, errors (*), trapped tiles (t), and incompletable configurations (inc). (*H*) Fat rhombs shaken alone. Moons (m) are now common and only one well-formed star (s) occurs. (*I–K*) XOR tiles, 1.2 cm on a side. (*I*) Four codes (c–f) are used. (*J*) Disaggregated. (*K*) Shaken ≈60 h. Note errors (*), incompletable configurations (inc), and triangles (Δ1, Δ2, Δ3). (*L*) A single mismatch may cause a dislocation (*) because mismatched edges are repulsive along 2/3 of their length. Structures in *L* were cropped from a larger image and lightened with Adobe Photoshop.

bonds. To enforce them, a four-patch WC (Fig. 3*E*) was used. Each rhomb was coated on two sides with a type a code and on two sides with a type b code (Fig. 3*E*, a and b). Rhombs were mixed in a ratio of $\approx\tau$:1 (fat/thin, $\tau = 1.618\ldots$, the golden mean) and disaggregated until no complete vertex star (arrangement of tiles around a vertex) occurred (Fig. 3*F*). After ≈9 days of shaking, large structures were observed (Fig. 3*G*). The structures had 716 ± 11 bonds ($n = 3$, 90% of the 800 bonds in a single decagonal IS), few mismatches 7.6 ± 7 (an error rate of 1%), and all eight kinds of vertex star present in a mathematical P tiling. However, the frequency at which each vertex star appeared did not agree with theory; e.g., consider the two vertex stars termed stars and moons (Fig. 3*G*, s and m). Stars and moons both are comprised of five fat rhombs but in a different arrangement: tiles in stars are connected by type a bonds, in moons by type b bonds. The observed ratio of stars/moons was 19:1 (57 stars and three moons total, $n = 3$) but the theoretical ratio for a P tiling is $\approx 2.6{:}1$ (τ^2:1, by methods in ref. 24).

A possible explanation for this discrepancy is that type a and type b bonds have different strengths. To check, fat rhombs were shaken alone (Fig. 3*H*) by using a similar, but shorter, annealing schedule (≈2 days). The observed ratio stars/moons (now the only possible vertex stars) was ≈1:5 (six stars and 25 moons total, $n = 3$). This reversal in ratio seems inconsistent with the results in Fig. 3*G*, but it can be understood by considering unbound edges. For Fig. 3*G* the ratio of unbound edges type a/type b is ≈2.3:1 (173 ± 16, 75 ± 8); for Fig. 3*H* this ratio is ≈1.3:1 (386 ± 4, 299 ± 8). In both cases minimizing the energy of the system left more unbound edges of type a; type b bonds are stronger. I ascribe this asymmetry to the number of wetting changes: type b edges have two more changes (and hence their menisci more area) than type a edges have. Independent of any difference in bond strengths one might expect that stars, in the presence of thin rhombs, are more stable than moons. The addition of five thin rhombs to a star yields a structure in which the star is greatly stabilized—four bonds must be broken before the star is destroyed. In contrast, 15 tiles must be added to a moon before it is similarly stabilized. The stabilization of stars by thin rhombs may be enhanced because thin rhombs bind stars by strong type b bonds.

XOR tile matching rules require four kinds of nonpalindromic bonds. To enforce them a six-patch WC (Fig. 3*I*, c–f) was used.

The WC was designed so that (*i*) every tile side had three F and three L patches to cancel the capillary forces' contribution to the position of the tile, (*ii*) every tile side had three or five changes in wetting character to help make all bonds isoenergetic, and (*iii*) if two sides with the correct geometry mismatched, they did so at four of six patches, giving the mismatch a net repulsive character. While the codes were nonpalindromic and could be used on square tiles with straight sides, shape complementarity was used to help differentiate the input and output sides of the tiles and prevent shifted bonds.

To show the specificity of the WC for XOR tiles, 256 tiles were disaggregated and shaken without an input tile for ≈60 h (Fig. 3*K*). An average of 362 ± 5.2 bonds ($n = 3$, 75% of the 480 bonds in a square IS) and 13.7 ± 3.8 mismatches formed (an error rate of 3.6%). The four bond types were nearly equally represented (80 ± 7:88 ± 1.2:99 ± 7.6:95 ± 3, c/d/e/f), showing that they were nearly isoenergetic. Errors held in place by a single bond often resulted in dislocations (Fig. 3*L*). Without an input tile, the XOR tiles' IS (Fig. 1*J*) features blue triangles of zeros of all sizes. Experimentally XOR tiles gave complete triangles of size 1, 2, and 3 (Δ1, Δ2, Δ3, Fig. 3*K*).

Nucleation of XOR tile assembly on a four-bit input tile failed; the association of tiles into corners (as in Fig. 1*K*) seemed hindered (after 1 day shaking typically 1–2 tiles bound the nucleus). Changing the shape of the tiles, making a flexible input tile, and increasing the rate of shaking in attempts (not shown) to increase the rate of association were unsuccessful. This raised the question: by what mechanism were the large structures observed in unnucleated experiments formed? To answer this, the formation of 275 bonds (present after 2 h shaking without an input tile) was observed by reversing a video of the assembly. Several observations were made. (*i*) The desired association mechanism occurred infrequently; few bonds (13.5%) resulted from the binding of a tile into a corner in any orientation and fewer still (5.5%) in the orientation required to fit in an input tile. (*ii*) Most bonds resulted from events involving two multi-tile structures (61.5%). (*iii*) Dimers were the major active species: 44.7% of all bonds resulted from the association of a dimer to a single tile or multi-tile structure. (*iv*) The simultaneous formation of two or more parallel bonds (e.g., dimerization of dimers to form a square tetramer) was the dominant growth mechanism, 51.6% of all bonds. Thus SA proceeded largely by the assembly of monomers into dimers via single bonds followed by the creation of larger structures via parallel associations.

Measurement of cooperative binding into corners was difficult because tiles bound them so infrequently, but the low error rate (2.8%, similar to longer experiments) and the observed association mechanism together suggest that binding was indeed cooperative. Consider association at a site comprised of two adjacent parallel edges. For such a site there are six dimers, two correct and four incorrect, that can bind. Without cooperativity to select one of the correct dimers, the error rate would be 1/3, i.e., for every two bonds formed, one would expect one mismatch to form. Because 45.8% of all bonds formed by such a mechanism one would expect an error rate ⩾18.6% (expected mismatches ⩾22.9% of bonds, recall % error = mismatches/[mismatches + bonds] = 22.9/122.9). Thus cooperativity appears responsible for an error rate ≈6-fold lower than expected assuming noncooperative binding.

These experiments show (*i*) that WCs can be used to enforce matching rules for a simple computation and (*ii*) that the binding of tiles (as dimers or larger species) is reasonably cooperative. The quality of experimental structures followed the trend observed in simulations; C tiles made the fewest errors (none), P tiles made more, and XOR tiles made the greatest number. These data support the hypothesis that features of a tile set (e.g., number of matching rules or whether it is competitive) impact the frequency of defect formation; to draw stronger conclusions future studies must compare the SA of different tile sets by using identical WCs and annealing schedules. The error rate for XOR tiles was high enough to preclude useful computation but not so high that expected features (triangles of zeros) could not be observed. Finally, quantitative details of bond equilibria and kinetics greatly influenced the structures formed. For P tile structures, the expected vertex stars were present but unequal bond strengths may have contributed to the unexpected vertex star statistics observed. For XOR tiles, an unexpectedly low rate of association into corners was observed; this limits the structures accessible by XOR tile SA to random computations. Finding systems where SA can be nucleated on an input tile is important for studying the full range of structures suggested by the connection of computation and SA.

I thank L. Adleman, E. Winfree, R. Lee, N. Seeman, N. Chelyapov, D. Fygenson, R. Mills, K. Casciotti, K. Bui, J. Lyons, and L. Bennett of Laser Connection, Arcadia, CA, and Flag's Photo of Pasadena, CA. This work was supported by grants from the Defense Advanced Research Projects Agency, the Sloan Foundation, the National Aeronautics and Space Administration/Jet Propulsion Laboratory, the Office of Naval Research, and the National Science Foundation.

1. Grünbaum, B. & Shephard, G. C. (1986) *Tilings and Patterns* (Freeman, New York).
2. Wang, H. (1963) in *Proceedings of the Symposium on Mathematical Theory of Automata*, ed. Fox, J. (Polytechnic, New York), pp. 23–56.
3. Levine, D. & Steinhardt, P. J. (1984) *Phys. Rev. Lett.* **53,** 2477–2480.
4. Adleman, L. M. (1994) *Science* **266,** 1021–1024.
5. Winfree, E., Liu, F., Wenzler, L. A. & Seeman, N. C. (1998) *Nature (London)* **394,** 539–544.
6. Winfree, E., Yang, X. & Seeman, N. C. (1998) in *DNA-Based Computers II*, eds. Landweber, L. F. & Baum, E. B. (Am. Math. Soc., Providence, RI), pp. 191–213.
7. Hosokawa, K., Shimoyama, I. & Miura, H. (1996) *Sens. Actuators A* **57,** 117–125.
8. Bowden, N., Terfort, A., Carbeck, J. & Whitesides, G. M. (1997) *Science* **276,** 233–235.
9. Bowden, N., Choi, I. S., Gryzbowski, B. A. & Whitesides, G. M. (1999) *J. Am. Chem. Soc.* **121,** 5373–5391.
10. Dimitrov, A. S., Dushkin, C. D., Yoshimura, H. & Nagayama, K. (1994) *Langmuir* **10,** 432–440.
11. Kralchevsky, P. A., Paunov, V. N., Denkov, N. D. & Nagayama, K. (1995) *J. Chem. Soc. Faraday Trans.* **91,** 3415–3432.
12. Markov, I. V. (1995) *Crystal Growth for Beginners* (World Scientific, Singapore), pp. 13–20.
13. Garg, A. & Levine, D. (1987) *Phys. Rev. Lett.* **59,** 1683–1686.
14. Penrose, R. (1978) *Eureka* **39,** 16–22.
15. Morita, K. (1992) *Inf. Proc. Lett.* **42,** 325–329.
16. Meakin, P. (1983) *Phys. Rev. Lett.* **51,** 1119–1122.
17. Elser, V. (1985) *Phys. Rev. Lett.* **54,** 1730.
18. Reif, J. (1999) in *DNA Computers III*, eds. Rubin, H. & Wood, D. H. (Am. Math. Soc., Providence, RI), pp. 217–254.
19. Onoda, G. Y., Steinhardt, P. J., DiVincenzo, D. P. & Socolar, J. E. S. (1998) *Phys. Rev. Lett.* **60,** 2653–2656.
20. Ronchetti, M., Bertagnolli, M. & Jarić, M. V. (1990) in *Geometry and Thermodynamics*, ed. Tolédano, J.-C. (Plenum, New York), pp. 141–158.
21. Winfree, E. (1998) Ph.D. thesis (California Institute of Technology, Pasadena).
22. Kralchevsky, P. A. & Nagayama, K. (1994) *Langmuir* **10,** 23–36.
23. Gaydos, J. & Neuman, A. W. (1996) in *Applied Surface Thermodynamics,* eds. Neuman, A. W. & Spelt, J. K. (Dekker, New York), pp. 169–238.
24. Senechal, M. (1995) *Quasicrystals and Geometry* (Cambridge Univ. Press, Cambridge).
25. Wolfram, S. (1994) *Cellular Automata and Complexity* (Addison–Wesley, New York).